J|A|C|S ARTICLES

Published on Web 11/17/2008

Manipulating Crystal Orientation in Nanoscale Cylindrical Pores by Stereochemical Inhibition

Benjamin D. Hamilton,[†] Isabelle Weissbuch,[§] Meir Lahav,[§] Marc A. Hillmyer,*[,‡] and Michael D. Ward*[,⊥]

Department of Chemical Engineering and Materials Science and the Department of Chemistry, University of Minnesota, Minneapolis, Minnesota 55455, Department of Materials and Interfaces, The Weizmann Institute of Science, 76100 Rehovot, Israel, and Molecular Design Institute, Department of Chemistry, New York University, 100 Washington Square East, New York, New York 10003-6688

Received September 10, 2008; E-mail: hillmyer@umn.edu; mdw3@nyu.edu

Abstract: Glycine nanocrystals, grown in aligned nanometer-scale cylindrical pores of nanoporous polystyrene-poly(dimethyl acrylamide) monoliths by evaporation of imbibed aqueous solutions, adopt preferred orientations with their fast-growth axes aligned parallel with the pore direction. X-ray diffraction analysis revealed the exclusive formation of the metastable β-polymorph, with crystal size comparable with the 22 nm pore diameter, in contrast to the formation of α-glycine in the absence of nanoscale confinement. When grown from aqueous solutions alone, the nanocrystals were oriented with their [010] and [0$\bar{1}$0] axes, the native fast growth directions of the (+) and (−) enantiomorphs of β-glycine, respectively, aligned parallel with the pore direction. In contrast, crystallization in the presence of racemic mixtures of chiral auxiliaries known to inhibit growth along the [010] and [0$\bar{1}$0] directions of the enantiomorphs produced β-glycine nanocrystals with their [001] axes nearly parallel to the pore direction. Enantiopure auxiliaries that inhibit crystallization along the native fast growth direction of only one of the enantiomorphs allow the other enantiomorph to grow with the [010] axis parallel to the cylinder. Collectively, these results demonstrate that crystal growth occurs such that the fast-growing direction, which can be altered by adding chiral auxiliaries, is parallel to the pore direction. This behavior can be attributed to a competition between differently aligned crystals due to critical size effects, the minimization of the surface energy of specific crystal planes, and a more effective reduction of the excess free energy associated with supersaturated conditions when the crystal grows with its fast-growth axis unimpeded by pore walls. These observations suggest that the β-glycine nanocrystals form by homogeneous nucleation, with minimal influence of the pore walls on orientation.

Introduction

Crystal habit, the shape adopted by a crystal as it matures, is strongly influenced by the crystallization environment during nucleation and growth.[1] Solvents and additives can affect crystal habit by binding to specific crystal faces, which slows growth along the direction perpendicular to the adsorbing face while permitting unimpeded growth along other crystallographic directions. Additives designed to serve as crystallization regulators, sometimes referred to as crystallization auxiliaries, also can influence polymorphism,[2,3] the ability of molecules to adopt multiple crystalline forms. Certain crystallization auxiliaries, specifically amino acids, can inhibit growth of α-glycine crystals to the extent that the β-glycine form is generated.[4] Furthermore, whereas β-glycine generated by the addition of ethanol to an aqueous solution of glycine typically forms needles coinciding with the [010] direction,[5,6] resulting in vanishingly small (010) faces, evaporation of glycine solutions containing certain amino acid auxiliaries affords β-glycine crystals as plates with large (010) faces.

Our laboratories have reported the crystallization of organic compounds in nanoscale pores of controlled porous glass (CPG) and aligned cylindrical pores of porous polymer monoliths fabricated from diblock and triblock polymers.[7−9] These investigations revealed that the sizes of the crystals embedded within the pores were comparable with the pore diameters and

[†] Department of Chemical Engineering and Materials Science, University of Minnesota.
[§] Weizmann Institute of Science.
[‡] Department of Chemistry, University of Minnesota.
[⊥] New York University.

(1) Mullin, J. W. *Crystallization*; Elsevier: Oxford, U.K., 2004.
(2) Bernstein, J. *Polymorphism in Molecular Crystals*; Oxford: New York, 2002.
(3) Weissbuch, I.; Leiserowitz, L.; Lahav, M. *Adv. Mater.* **1994**, *6*, 952–956.
(4) Weissbuch, I.; Torbeev, V. Yu.; Leiserowitz, L.; Lahav, M. *Angew. Chem., Int. Ed.* **2005**, *44*, 3226–3229.
(5) Torbeev, V. Yu.; Shavit, E.; Weissbuch, I.; Leiserowitz, L.; Lahav, M. *Cryst. Growth. Des.* **2005**, *5*, 2190–2196.
(6) (a) Iitaka, Y. *Acta Crystallogr.* **1960**, *13*, 35–45. (b) Ferrari, E. S.; Davey, R. J.; Cross, W. I.; Gillon, A. L.; Towler, C. S. *Cryst. Growth Des.* **2003**, *3*, 53–60.
(7) Ha, J.-M.; Wolf, J. H.; Hillmyer, M. A.; Ward, M. D. *J. Am. Chem. Soc.* **2004**, *126*, 3382–3383.
(8) Ha, J.-M.; Hillmyer, M. A.; Ward, M. D. *J. Phys. Chem. B* **2005**, *109*, 1392–1399.

 10.1021/ja807193s CCC: $40.75

that polymorph selectivity during crystallization and polymorph stability rankings were affected by pore size. This behavior, which has been corroborated by others in studies of acetominophen crystallization in CPG,[10,11] can be attributed to the increasing importance of surface free energy compared with volume free energy as crystal size is reduced. Using X-ray microdiffraction, we also found that nanocrystals embedded in the porous polymer monoliths often exhibit preferred orientations with respect to the direction of the aligned pores.[7−9]

Recently, we demonstrated that glycine crystallization in the nanopores of CPG and porous polystyrene-poly(dimethyl acrylamide) monoliths (p-PS-PDMA) resulted in exclusive formation of the β-polymorph under conditions that generate α-glycine when crystallization is performed in bulk.[12] The β-glycine nanocrystals embedded in either matrix were remarkably stable. In CPG this form persisted well above the bulk $\beta \rightarrow \alpha$ phase transition temperature ($T_{\beta\rightarrow\alpha} = 67$ °C), melting near 180 °C. In p-PS-PDMA, the β-glycine nanocrystals converted to α-glycine only upon heating beyond the glass transition temperature of polystyrene ($T_g \approx 100$ °C). Numerous reports have described the crystallization of various materials within nanopores,[13] but only one system has addressed crystal alignment, finding that polymer crystals tend to grow with their fast-growth direction aligned parallel to the confining walls of one-dimensional pores ($\approx$35 nm diameter) in porous alumina.[14] Herein we describe the effect of confinement on the orientation of β-glycine nanocrystals grown in the one-dimensional pores of p-PS-PDMA and the role of crystallization auxiliaries on orientation. In the absence of auxiliaries, the β-glycine nanocrystals grow with their native fast-growth direction (i.e., the crystallographic *b* axis) parallel to the pore direction. The introduction of a racemic mixture of chiral auxiliaries known to block growth through enantioselective binding to the (010) faces, which are perpendicular to the native fast-growth direction, produces a different preferred orientation. In this case, crystal growth occurs along a direction that is not impeded by the pore walls or the auxiliary. Interestingly, the *b*-axis is parallel to the pore axis when only one of the enantiopure chiral auxiliaries is present, confirming that a single enantiomer binds to the fast growing end of only one of the β-glycine enantiomorphs.

Experimental Procedures

Materials and Methods. All reagents and solvents were used as received unless otherwise noted. Glycine was purchased from Sigma-Aldrich, Inc. (St. Louis, Missouri). Aqueous glycine solutions were passed through a 0.45 μm poly(tetrafluoroethylene) syringe filter before use to remove any insoluble particulate matter. Polylactide-poly(dimethyl acrylamide)-polystyrene (PLA-PDMA-PS) triblock polymers and monoliths were prepared according to procedures described in a previous report.[12] PLA-PDMA-PS triblocks were synthesized with volume fractions of $f_{PLA} = 0.30$, $f_{PDMA} = 0.13$, $f_{PS} = 0.57$, which were conducive to the formation of a hexagonally packed cylinder structure. When shear oriented, these triblock copolymers generated aligned cylinders of PLA, which were etched in base (1 M NaOH solution in 50:50 MeOH/H_2O) at 60 °C for 5 days to generate porous PS-PDMA (p-PS-PDMA) monoliths with cylindrical pores having 22 nm diameters. The p-PS-PDMA monoliths were dried under vacuum at room temperature for 3 h to remove residual water after postetch rinsing. The cylindrical pores in the p-PS-PDMA monoliths were well ordered, as confirmed by small-angle X-ray scattering. The interior lining of the pores was PDMA-rich and therefore hydrophilic, which permitted infiltration of aqueous solutions.

Crystallization in Nanoporous Block Copolymers. The p-PS-PDMA monoliths (approximately 1 mm × 2 mm cross-section and 3 mm along the pore direction) were immersed in water for 2 h prior to imbibing glycine solutions. This pretreatment was found necessary for consistent loading of glycine in the pores, as surmised from the Bragg peak intensity in the XRD. The monolith pieces were subsequently immersed in 18% glycine solution for 2 h, during which the glycine solution migrates into the pores of the monolith. After removal from solution, the outer surfaces of the monoliths were carefully swabbed with a soft dampened tissue to remove any external glycine solution residue. The monoliths were then dried under vacuum at approximately 0.1 mmHg for 4 h, although nanocrystals were detected by X-ray microdiffraction (see below) within 30 min. Further drying under vacuum did not affect the crystallization outcome, and allowing the monoliths to dry under ambient conditions afforded identical results but nanocrystals were not detected until after approximately 2 h. Further crystallization was evident during the next hour of drying.

Characterization. Wide-angle X-ray scattering microdiffraction (μ-XRD) was performed on a Bruker AXS (Madison, Wisconsin) microdiffractometer equipped with a 2D Siemens multiwire area detector and a 0.8 mm beam collimator. The full width at half-maximum (fwhm) resolution of the instrument was determined by measuring the fwhm for both a single crystal LaB_6 wafer and a single crystal of highly oriented pyrolytic graphite (HOPG). The fwhm resolution of the instrument was approximately 0.27° (2θ) over the 2θ range of 15°−35°, allowing for a maximum crystal size estimate of 30 nm by the Scherrer equation. Simulated X-ray powder patterns for α-, β-, and γ-glycine were generated using Mercury (Cambridge Crystallographic Data Center, Cambridge, United Kingdom, version 1.4.1) with crystallographic parameters obtained from the Cambridge Structural Database (Cambridge Crystallographic Data Center, Cambridge, United Kingdom).

The monoliths were affixed at the end of a brass pin using a small amount of clay such that striations on the monolith surface, known to be parallel with the direction of the pores, were parallel with the brass pin. The brass pin was then inserted into a sample holder supplied by the manufacturer and then tightened with a small screw. This sample was then mounted on a four-circle Eulerian cradle such that the cylindrical pores were aligned parallel with the X-ray detector, and then the cradle was adjusted via the instrument controls until the pores were aligned with the vertical centerline of the detector. A laser-video alignment system supplied by the manufacturer was used to determine whether the monolith was aligned with the beam, and the position of the brass pin was adjusted with small screws in the sample holder until the alignment system indicated the monolith was in the beam path. To verify the pores were aligned parallel with the vertical centerline of the detector, an initial set of X-ray data was collected and the azimuthal positions of the resulting Bragg reflections were observed. Proper

(9) Ha, J.-M. Crystallization and Thermotropic Properties of Organic Solids in Nanoscopic Reactors. Ph.D. Thesis. University of Minnesota, Minneapolis, MN, 2005.
(10) Beiner, M.; Rengarajan, G. T.; Pankaj, S.; Enke, D.; Steinhart, M. *Nano Lett.* **2007**, *7*, 1381–1385.
(11) Rengarajan, G. T.; Enke, D.; Steinhart, M.; Beiner, M. *J. Mater. Chem.* **2008**, *18*, 2537–2539.
(12) Hamilton, B. D.; Hillmyer, M. A.; Ward, M. D. *Cryst. Growth Des.* **2008**, *8*, 3368–3375.
(13) (a) Jackson, C. L.; McKenna, G. B. *J. Chem. Phys.* **1990**, *93*, 9002–9011. (b) Ajayan, P. M.; Iijima, S. *Nature* **1993**, *361*, 333–334. (c) Prasad, R.; Lele, S. *Phil. Mag. Lett.* **1994**, *70*, 357–361. (d) Patrick, W. A.; Kemper, W. A. *J. Phys. Chem.* **1938**, *42*, 369–380. Borisov, B. F.; Charnaya, E. V.; Hoffmann, W. D.; Michel, D.; Shelyapin, A. V.; Kumzerov, Yu. A. *J. Phys.: Condens. Matter* **1997**, *9*, 3377–3386. (d) Buffat, Ph.; Borel, J.-P. *Phys. Rev. A* **1976**, *13*, 2287–2298. (e) Reinnie, G. K.; Clifford, J. *J. Chem. Soc., Faraday Trans. 1* **1977**, *73*, 680–689. (f) Christenson, H. K. *J. Phys: Condens. Matter* **2001**, *13*, R95–R133.
(14) (a) Steinhart, M.; Göring, P.; Dernaika, H.; Prabhukara, M.; Gösele, U.; Hempel, E.; Thurn-Albrecht, T. *Phys. Rev. Lett.* **2006**, *97*, 027801. (b) Steinhart, M.; Stephan, S.; Wehrspohn, R. B.; Gosele, U.; Wendorff, J. H. *Macromolecules* **2003**, *36*, 3646–3651.

Scheme 1. Configuration for Diffraction Using the μ-XRD Equipped with a 2D Detector[a]

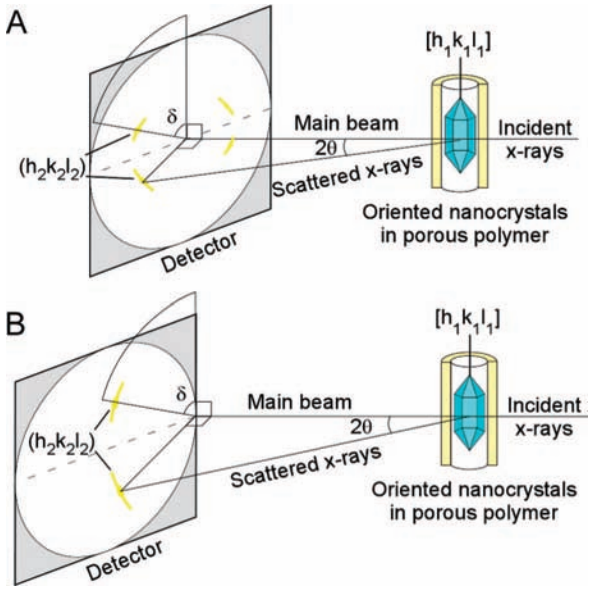

[a] The nanoporous monolith with embedded nanocrystals (depicted here as only a single cylinder) is held in a fixed orientation with respect to the detector, with the beam targeted at either the (A) center or (B) right edge of the detector. Reflections from specific crystal planes produce diffraction spots on the 2D detector at coordinates of $(2\theta, \delta)$, where 2θ is the Bragg diffraction angle and δ is the azimuthal angle on the detector that reflects the orientation of that plane with respect to $\delta = 0°$, which coincides here with the pore axis (the normal setting for experiments described herein). Arcs of intensity (rather than discrete points) signify a distribution of orientations of the reflecting plane about the preferred orientation.

alignment of the sample was evident when the reflections were symmetric about $\delta = 90°$, which verified that crystals pointed in opposite directions within the pores were also symmetric about $\delta = 90°$. This indicated the pores were parallel with the vertical center, and if the data suggested otherwise, the Eulerian cradle was adjusted with the instrument controls until the Bragg reflections from the monolith met this criteria.

Data were collected in a forward scattering mode, initially with the monolith aligned parallel with the vertical center line of the detector ($\delta = 0°$) and the incident X-ray beam centered on the detector (Scheme 1A). The sample-to-detector distance was 6 cm. In this configuration, Bragg reflections were collected over a full azimuthal circle ($0° \leq \delta \leq 360°$) with radius $0° \leq 2\theta \leq 30°$ (Scheme 1A). Data also were collected at a sample-to-detector distance of 15 cm and the monolith positioned parallel to the right edge of the detector ($\delta = 0°$; Scheme 1B). Many reflections were more readily discerned at the longer sample-to-detector distance, although this configuration precluded data collection spanning the entire 360° azimuth. Instead, Bragg reflections were collected over the quadrant of the full-circle ranging from $2.5° \leq 2\theta \leq 37.5°$ and $45° \leq \delta \leq 135°$. Rotation of the monoliths counterclockwise about the δ-axis by 90°, such that $\delta = 0°$ was coincident with the horizon of the detector, allowed data collection ranging from $2.5° \leq 2\theta \leq 37.5°$ and $-45° \leq \delta \leq 45°$, which was equivalent to the top quadrant of the full circle. Data collection for the two remaining quadrants was not necessary as these are simply mirror images of the left and top quadrants.

Results

Aligned 1D Crystallization Nanoreactors. Nanoporous PS-PDMA monoliths were fabricated by chemical etching of the PLA block of shear oriented monolith of a PS-PDMA-PLA triblock polymer (PS = polystyrene; PDMA = poly(dimethyl acrylamide); PLA = poly(lactide))[15] prepared with volume fractions of $f_{PLA} = 0.30$, $f_{PDMA} = 0.13$, $f_{PS} = 0.57$. This composition was conducive to the formation of hexagonally packed cylinders of PLA in the PS matrix, and etching produced aligned empty cylinders with hexagonal order in the PS matrix. Nuclear magnetic resonance (NMR) analysis confirmed ≥99% removal of the PLA with retention of the PDMA, which lined the interior walls of the pores. Scanning electron microscopy (SEM) of the etched monoliths revealed a hexagonal array of cylindrical pores with 20 nm diameters oriented parallel to the direction of triblock alignment (Figure 1A). The PDMA lining imparted a hydrophilic character to the cylinder walls, enabling penetration of aqueous solutions. Recently, we capitalized on this property by filling the cylindrical pores with an undersaturated aqueous glycine solution by immersion of the monolith in the solution.[12] After removal from the solution in which the monolith was immersed, subsequent evaporation of the water from the cylindrical pores resulted in the formation of glycine nanocrystals confined within the nanopores, exclusively as the metastable β-polymorph (Figure 1B). The selectivity for β-glycine was attributed to a size-dependent polymorph stability crossing, as only α-glycine is observed under the same conditions when crystallized in bulk.[16] The influence of size was corroborated by the selectivity for β-glycine in the nanopores of controlled porous glass (CPG), with β-glycine observed in pore sizes that ranged from 7.5 to 55 nm.

Unlike CPG, the uniformity of the nanopores in the p-PS-PDMA monoliths and their high degree of alignment presents an opportunity to explore in detail the influence of the anisotropic 1D environment of the nanopores on crystal growth. As reported previously, individual monoliths, with the pores in a fixed orientation, can be interrogated by X-ray microdiffraction, enabling determination of the correspondence between the nanocrystal and pore orientations.[7−9] The large number of pores in a 1 mm × 1 mm × 2 mm monolith ($>10^9$) ensures that the number of crystals formed is sufficiently large that the X-ray data is effectively a powder pattern of the embedded crystals with random orientations about the pore axis while allowing determination of the crystal orientation with respect to the pore direction. Accurate determinations of nanocrystal orientation, however, requires that the alignment of the nanopores is sufficiently uniform. Prior to etching, small-angle X-ray scattering (SAXS) of the aligned triblocks revealed Bragg peaks consistent with hexagonally packed PLA cylinders with diameters of 22 ± 2 nm, where the error corresponds to the pore diameters expected at $q^* \pm \sigma$ (σ = one standard deviation of the intensity distribution about q^*). These cylinders are surrounded by a PDMA lining (approximately 1.7 nm thick, based on the PDMA volume fraction) and a PS matrix. The extent of cylinder orientation in the triblock monoliths, as given by the second order orientation factor F_2 (eq 1), was determined from the 2-D SAXS data using the normalized orientation distribution function $P(\phi)$ (eq 2), where ϕ is the azimuthal angle around a circle of constant q and $I(q^*,\phi)$ is the scattering intensity at the

(15) (a) Rzayev, J.; Hillmyer, M. A. *Macromolecules* **2005**, *38*, 3–5. (b) Rzayev, J.; Hillmyer, M. A. *J. Am. Chem. Soc.* **2005**, *127*, 13373–13379.

(16) (a) Boldyreva, E. V.; Drebushchak, V. A.; Drebushchak, T. N.; Paukov, I. E.; Kovalevskava, Y. A.; Shutova, E. S. *J. Therm. Anal. Calorim.* **2003**, *73*, 409–418. (b) Boldyreva, E. V.; Drebushchak, V. A.; Drebushchak, T. N.; Paukov, I. E.; Kovalevskava, Y. A.; Shutova, E. S. *J. Therm. Anal. Calorim.* **2003**, *73*, 419–428. (c) Chongprasert, S.; Knopp, S. A.; Nail, S. L. *J. Pharm. Sci.* **2001**, *90*, 1720–1728.

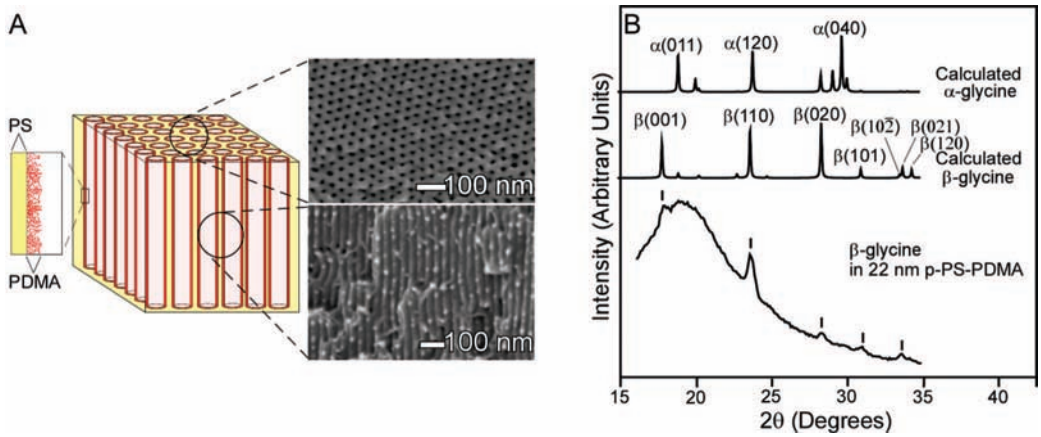

Figure 1. (A) Schematic representation (left) and SEM images (right) of a p-PS-PDMA monolith produced by chemical etching of PLA from shear-aligned p-PS-PDMA-PLA triblock copolymers. The SEM images are views parallel (top) and perpendicular (bottom) to the cylinder axes. The pores exhibit hexagonal order and diameters consistent with those determined by SAXS (22 ± 2 nm). The spherical features in the bottom SEM figure are attributed to plastic deformation of the PS matrix due to shear stresses occurring during fracture of the monolith. (B) 1D XRD data for β-glycine nanocrystals embedded within p-PS-PDMA monoliths with 22 nm pores. The diffraction peaks are superimposed on diffuse scattering from the amorphous polymer matrix. Comparison of the data with the simulated powder diffraction patterns, based on the known single crystal structures for α- and β-glycine, confirms the exclusive formation of β-glycine in the nanopores.

primary Bragg peak, q^*.[17] Typically, $F_2 \approx 0.92$ (eq 2) for the PS-PDMA-PLA monoliths.[18,19] Monoliths with F_2 values in the range $0.8 \leq F_2 \leq 0.9$ were obtained occasionally, but the apparent nanocrystal orientation measured by X-ray microdiffraction, which relies on uniform alignment of the pores, decreased with decreasing F_2. Monoliths with $F_2 < 0.8$ were completely unsuitable due to highly nonuniform orientation of the pores. Therefore, only monoliths with $F_2 \approx 0.92$ were used for chemical etching and subsequent investigations of nanocrystal orientation. SAXS measurements of the p-PS-PDMA monoliths obtained after chemical etching of the PLA block confirmed retention of the alignment, with $F_2 \approx 0.92$. The cylinder diameter inferred from the SAXS data is equivalent, within error, to the 20 nm diameter measured by SEM, which is reduced from the actual value by the platinum coating (Figure 1).

$$F_2 = 1 - 3\langle(\cos\theta)^2\rangle\langle(\cos\theta)^2\rangle = \int_0^{\pi} (\cos\theta)^2 P(\phi) \sin\phi \, d\phi \quad (1)$$

$$P(\phi) = \frac{I(q^*, \phi)\, q^{*2}}{\int_0^{\pi} I(q^*, \phi)\, q^{*2} \sin\phi \, d\phi} \quad (2)$$

Crystallization of β-Glycine Nanocrystals. The crystallization of β-glycine in the nanopores of p-PS-PDMA is particularly interesting because of the unique crystallographic characteristics of this polymorph and the influence of certain additives on its growth. Macroscopic β-glycine grows as needles (typically 500 μm long and 25 μm in diameter) from alcohol/water solutions,[6] crystallizing in the $P2_1$ space group with $a = 5.077$ Å, $b = 6.268$ Å, $c = 5.38$ Å, and $\beta = 113.2°$. The long axis of the needles coincides with the [010] direction of the crystal (b-axis). The $P2_1$ space group is chiral and β-glycine exists as two polar enantiomorphs, (+)-β and (−)-β. Because the crystals are polar, each enantiomorph is characterized by one end that grows more rapidly than the other. Previous attempts to assign the polarity of individual crystals via the Bijvoet method were unsuccessful owing to the weak anomalous scattering of the constituent atoms in glycine and the near-centrosymmetry of the crystals;[5] therefore, the individual enantiomorphs were assigned according to the direction of the glycine C−H bonds: the enantiomorph with the C−H bonds protruding from the (010) face was defined as (+)-β, whereas the enantiomorph with the C−H bonds protruding from the (0$\bar{1}$0) face was defined as (−)-β, as required by symmetry. The enantiomorphs were discerned experimentally by the effect of chiral amino acid additives on growth, wherein *R*-amino acids bound selectively to the (010) face of (+)-β and *S*-amino acids to the (0$\bar{1}$0) face of (−)-β (Figure 2).[20,21] In each case, the additives significantly attenuated crystal growth by binding to the face at the fast-growing end. On the basis of the action of the chiral additives, the fast-growing end was assigned to the face with exposed C−H groups. That is, in the absence of additives (+)-β glycine grows rapidly along the $+b$ direction, or [010], and (−)-β-glycine grows rapidly along the $-b$ direction, or [0$\bar{1}$0]. By extension, the addition of an *R*-amino acid will suppress the growth of (+)-β with no significant impact on the growth of (−)-β glycine, whereas the opposite will occur upon addition of an *S*-amino acid. In this respect, *R*- and *S*-Trp, *R*- and *S*-Phe, and *R*- and *S*-Met (Trp = tryptophan; Phe = phenylalanine; Met = methionine) were particularly effective growth inhibitors.

Glycine was crystallized within the aligned cylinders of the p-PS-PDMA monoliths by evaporating the water from the imbibed aqueous solutions. The exterior surfaces of the mono-

(17) Sakurai, S.; Aida, S.; Okamoto, S.; Ono, T.; Imaizumi, K.; Nomura, S. *Macromolecules* **2001**, *34*, 3672–3678.

(18) (a) Zalusky, A. S.; Olayo-Valles, R.; Taylor, C. J.; Hillmyer, M. A. *J. Am. Chem. Soc.* **2001**, *123*, 1519–1520. (b) Zalusky, A. S.; Olayo-Valles, R.; Wolf, J. H.; Hillmyer, M. A. *J. Am. Chem. Soc.* **2002**, *124*, 12761–12773. (c) deGennes, P. G.; Prost, J. *The Physics of Liquid Crystals*; Oxford University Press: New York, 1993. (d) Sakurai, S.; Aida, S.; Okamoto, S.; Ono, T.; Imaizumi, K.; Nomura, S. *Macromolecules* **2001**, *34*, 3672–3678.

(19) Additional monoliths were obtained with the same nominal pore size and F_2 values between 0.8 and 0.9. The orientation of glycine nanocrystals embedded within these monoliths was evident in m-XRD, but the degree of this orientation decreased as F_2 decreased. Below $F_2 \approx 0.8$, nanocrystal orientation was not observed.

(20) Weissbuch, I.; Lahav, M.; Leiserowitz, L. *Cryst. Growth Des.* **2003**, *3*, 125–150.

(21) Weissbuch, I.; Leiserowitz, L.; Lahav, M. *Chirality* **2008**, *20*, 736–748.

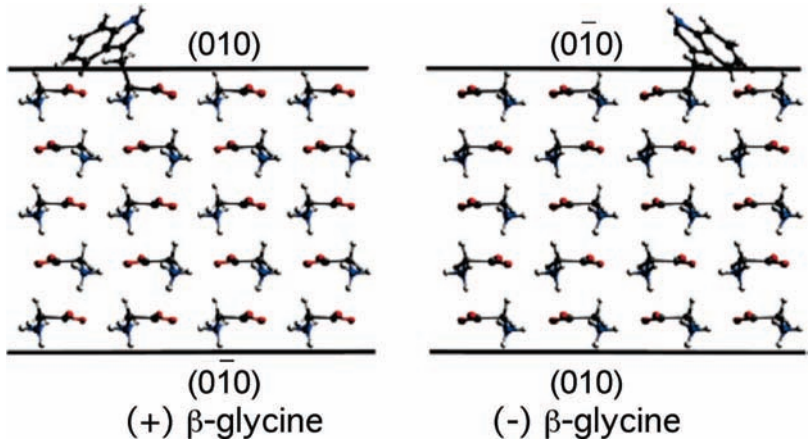

Figure 2. Molecular packing in the two enantiomorphs of β-glycine as viewed parallel to the (010) and (0$\bar{1}$0) planes, depicted with a *R*-Trp and *S*-Trp binding to the (010) and (0$\bar{1}$0) surfaces, respectively. Adapted from ref 5. Copyright 2005 American Chemical Society.

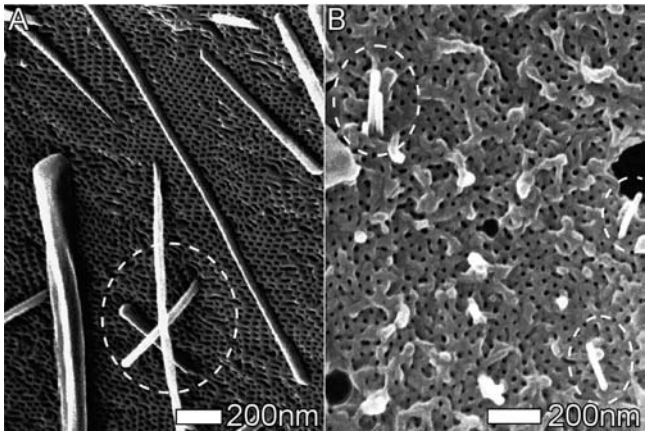

Figure 3. SEM images of β-glycine nanocrystals upon the outer surface of a p-PS-PDMA monolith after evaporation of an aqueous glycine solution containing (A) 18% glycine (w/w water) and (B) 18% glycine and 1.2% (w/w water) *R*,*S*-phenylalanine auxiliary prior to swabbing. The circled regions contain glycine nanocrystals protruding from the monolith pores. Long β-glycine needles laying flat on the monolith surface also are observed in panel A. The bright irregular features in panel B are attributed to plastic deformation of the PS matrix during fracture of the monolith. The diameters of the crystals appear larger than the pore diameters, which likely reflects maturation of the crystals protruding from the pores as the aqueous glycine solution evaporates.

liths were subsequently swabbed with a damp cloth to remove any extraneous crystals or residue, which were evident from SEM images of some unswabbed monoliths. Some crystals were found to lay flat on the surface of the exposed cylindrical pores, whereas other crystals protruded from the pores (circled, Figure 3A). This crystal habit is unlike that observed on the sides of the unswabbed monoliths or on nonporous substrates, where α-glycine is observed. This suggests that these needles, which have the customary habit of β-glycine, grew out of the monolith during solvent evaporation from β-glycine nanocrystals embedded just beneath some of the pore entrances, then collapsed across the surface during handling. On the basis of the concentration of the glycine solution, the density of β-glycine, and complete filling of the pores, approximately 14% of the pore volume should be filled by crystals.[22] The SEM images suggest that crystals emanate from roughly 1% of the pores exposed at the surface. Several of the monoliths were cooled in liquid nitrogen and cut with a razorblade at a depth of approximately 0.1 mm below the exposed porous surface. No crystals were evident in SEM images of newly exposed surfaces, which could reflect the small loading of glycine within the monolith. We note that similar difficulties were encountered in attempts to visualize cadmium sulfide particles embedded in nanoporous polystyrene monoliths.[23]

The nanocrystals embedded in the highly aligned cylindrical nanopores of the p-PS-PDMA monoliths were characterized by wide-angle X-ray microdiffraction (μ-XRD) using a 2-D area detector. These nanocrystals produced Bragg reflections at $2\theta = 17.9°$, $23.8°$, $28.4°$, $31.1°$, and $33.8°$, consistent with β-glycine, superimposed on background scattering due to the monolith (Figure 1B).[24] The peak widths corresponded to crystal sizes commensurate with the 22 nm pore diameter. The 2-D μ-XRD data, which were collected as a full circle ($0° \le \delta \le 360°$) at values of $0° \le 2\theta \le 30°$, contained bright spots near the beam stop at azimuthal angles of $\delta = 90°$ and $270°$ (with δ measured from the top of the circle) caused by small-angle scattering from the monolith cylinders, which were aligned parallel to $\delta = 0°$. Although careful inspection of the 2D scattering pattern revealed $\beta(020)$ reflections at $\delta = 0°$ and $180°$ (Figure 4A), other reflections were difficult to detect among the background scattering. Additional reflections could be discerned, however, by increasing the sample-to-detector distance so that diffraction data was collected for only one quadrant of the full-circle at a time, specifically for the left ($45° \le \delta \le 135°$; Figure 4C,D) and top ($-45° \le \delta \le 45°$; Figure 4E,F) quadrants. Data collection for the two remaining quadrants was not necessary as these were simply mirror images of the left and top quadrants. This configuration permitted collection of Bragg reflections at values of $2.5° \le 2\theta \le 37.5°$. The reflections appeared as arcs with well-defined intensity maxima, located at specific azimuthal angles (i.e., δ). The observation of intensity across a range of δ values rather than discrete points indicates that the nanocrystals adopt a statistical distribution of orienta-

(22) Based on an aqueous 18% (w/w water) glycine solution and a glycine density of $\rho = 1.16$ g/mL.

(23) Johnson, B. J. S.; Wolf, J. H.; Zalusky, A. S.; Hillmyer, M. A. *Chem. Mater.* **2004**, *16*, 2909–2917.

(24) Comparison of 1-D powder patterns generated from the 2-D m-XRD data with patterns generated from the known glycine crystal structures indicated that β-glycine was the exclusive polymorph for ~90% of the samples; the remainder contained α-glycine. Analysis of the peak widths by the Scherrer equation (see: Cullity, B. D. Elements of X-ray Diffraction; Addison-Wesley: Reading, MA, 1978.) produced β-glycine crystal size estimates of 22 nm, consistent with the 22 nm pore diameter of the p-PS-PDMA.

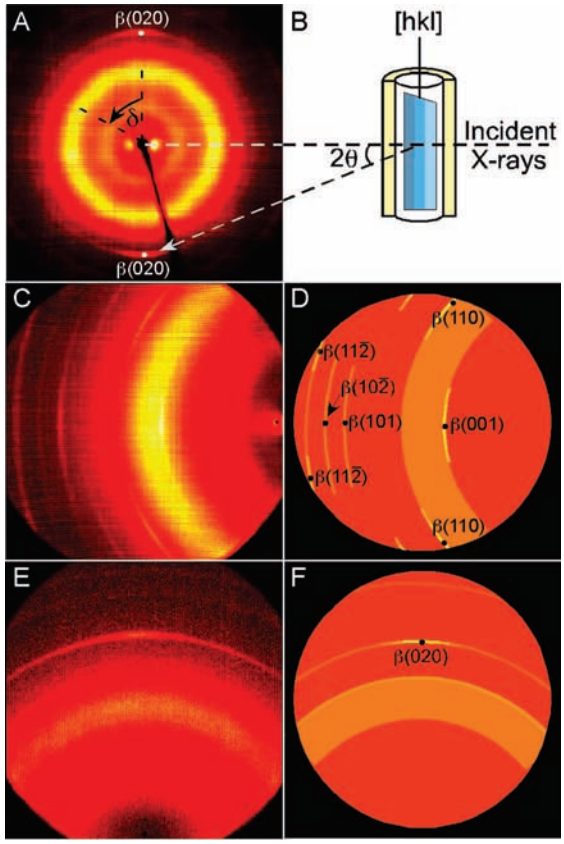

Figure 4. (A) Diffraction pattern observed on the 2D detector for β-glycine nanocrystals embedded in a 22-nm p-PS-PDMA monolith with its cylindrical pores parallel to the vertical axis at $\delta = 0$, as depicted in panel B. (C) The left quadrant of the 2D detector ($45° \leq \delta \leq 135°$) revealing arcs of intensity due to Bragg reflections. (D) A schematic enhancing the reflection positions and locations of maximum intensity in panel C with the corresponding assignments. (E) The top quadrant of the 2D detector ($-45° \leq \delta \leq 45°$) with the monolith fixed in the same configuration and (F) a schematic enhancing the reflection positions and locations of maximum intensity in panel E, with the corresponding assignments. The azimuthal angles (δ) of the Bragg reflections are consistent with preferential orientation of the {010} axis of β-glycine parallel to the pore direction. The schematics D and F, which were constructed using the raw data as a guide, are intended to clarify the positions of the Bragg reflections and their assignments. The black dots denote the azimuthal angle corresponding to maximum intensity. Some reflections exhibit intensity maxima at two azimuthal angles, related by symmetry, corresponding to opposite orientations of the crystals in the monolith pores (see Table 1).

tions about an average preferred orientation (the intensity maximum) with respect to the cylinder axis. The (001), (110), and (020) reflections were sufficiently intense for accurate analysis of the intensity distribution with respect to δ, which revealed that 95% of the intensity was contained within $65° \leq \delta \leq 115°$, $43° \leq \delta \leq 67°$, and $-20° \leq \delta \leq 20°$, respectively.

The orientation of the nanocrystals can be determined from the positions of the Bragg reflections ($h_2k_2l_2$), as given by the coordinates (2θ, δ) on the 2D detector, by calculating the angle (ϕ) between the Miller plane ($h_2k_2l_2$) and the Miller plane $(h_1k_1l_1)_\perp$ perpendicular to the pore direction (eq 3a). The identity of $(h_1k_1l_1)_\perp$ can be determined by trial-and-error, calculating the interplanar angles between ($h_2k_2l_2$) planes and trial values of $(h_1k_1l_1)_\perp$ until a self-consistent set of ϕ values that agrees with the data is obtained. The crystallographic direction parallel to pore direction can be defined as perpendicular to $(h_1k_1l_1)_\perp$. When applied to the scattering data in Figure 4C (Table 1), this analysis revealed unambiguously that the (020) planes were perpendicular

Table 1. Measured and Expected Bragg Reflection Parameters for β-Glycine Nanocrystals Embedded within p-PS-PDMA Monoliths, Based on The [010] Crystal Axis Coinciding with the Cylindrical Pores

	measured				expected		
reflection (*hkl*)	2θ (deg)	δ (deg)[a]	cos θ cos δ	ϕ (deg)[b]	2θ (deg)	ϕ (deg)[c]	δ (deg)[a,b]
(001)	17.9	90	0.00	90	17.9	90	90
(110)	23.8	55, 125	0.56	56	23.8	53	52, 128
(020)	28.5	0[d]	0.97	14[d]	28.5	0[d]	*d*
(101)	31.1	90	0.00	90	31.1	90	90
(10$\bar{2}$)	33.7	90	0.00	90	33.7	90	90
(021)	33.8	30, 150	0.83	34	33.8	32	28, 152
(120)	34.4	30, 150	0.83	34	34.4	34	30, 150
(002)	33.6	90	0.00	90	36.3	90	90
(11$\bar{2}$)	36.6	70, 110	0.32	71	36.7	67	65, 115

[a] Reflections appearing as pairs of δ values symmetrically opposed across $\delta = 0°$ and 90° can be attributed to glycine nanocrystals oriented in opposite directions within the pores. [b] Calculated using eq 3a. [c] Calculated with (*hkl*) and (010) assuming [010] parallel with the pore direction. [d] ϕ (from measured) is the *apparent angle between* (*hkl*) and (010), the plane perpendicular to the pore direction. The (020) is perpendicular to [010], and only forward scattering would be expected from this plane, that is there would be no reflection for the (020). The crystals are not all perfectly aligned, however, and the small fraction of crystals oriented such that their (020) is tilted $(2\theta/2) = \theta = 14.25°$ relative to the beam satisfy the Bragg condition. This leads to the appearance of the (020) reflection at $\delta = 0°$, which corresponds to an *apparent* $\phi = \theta = 14.25°$.

to the cylinder axis. Given the monoclinic symmetry of β-glycine, whereby the [010] and (020) are perpendicular, the embedded nanocrystals are preferentially oriented with the [010] axis, *the native fast growth direction*, aligned with the pore direction.

The deduction of [010] as the crystallographic axis coinciding with the pore direction was corroborated by the diffraction pattern observed on the top quadrant, which exhibited an arc at $2\theta = 28.5°$, consistent with the (020) reflection. Crystals aligned with the (010) plane perpendicular to the pore-direction and parallel to the incident X-ray beam ordinarily would not produce Bragg reflections from any (*hkl*) when $h = 0$ *and* $l = 0$, as only forward scattering would be observed on the detector. Under this condition, however, (*hkl*) with only $h = 0$ *or* only $l = 0$ will produce Bragg reflections on the detector if they are allowed by symmetry. The observation of a (020) reflection at $2\theta = 28.5°$ can only be explained by the existence of a small fraction of the crystals (f_θ) that are tilted relative to the beam by $\theta = 14.25°$, such that the Bragg condition is fulfilled for their (020) planes. Because these f_θ crystals have their (020) tilted relative to the beam by $\theta = 14.25°$, the measured θ and δ values produce an apparent $\phi_{app} = \theta = 14.25°$ (eq 3a, Table 1). It is important to note that this ϕ_{app} is solely due to diffraction by the f_θ crystals and not crystals in the preferred orientation, which do not produce reflections because they do not meet the Bragg condition. The azimuthal spread of the (020) reflection containing 95% of the total intensity was $-20 \leq \delta \leq 20°$, indicating a compact angular distribution of these crystals about the beam axis. The maximum of the azimuthal intensity is located at $\delta = 0°$, which argues that, of the crystals described by f_θ, most are rotated about the beam axis by only a small amount. Because the pores have cylindrical symmetry, one would expect the δ spread to be comparable to $\theta = 14.25°$, the tilt observed for a measureable fraction of the crystals. Indeed, analysis of the azimuthal intensity distribution reveals a Gaussian profile for the (020) reflections with 99% of the intensity confined within an angular spread of $-29° \leq \delta \leq 29°$, suggesting a range of

crystal orientations comparable to the tilt of the f_θ crystals. Notably, crystals aligned with (020) in this range could achieve lengths as large as 44 nm along ⟨010⟩, the fast growth direction. Crystals oriented outside this angular range would be more constrained along ⟨010⟩, which could prohibit crystals thus aligned from achieving critical size.

$$\Phi = \cos^{-1}(\cos\theta\cos\delta) \tag{3a}$$

$$\delta = \cos^{-1}\left(\frac{\cos\Phi}{\cos\theta}\right) \tag{3b}$$

The observation of a preferred orientation argues against the instantaneous formation of randomly oriented nuclei that retain their initial orientation and grow uniformly. Instead, the observations are consistent with (i) a preferred orientation of the crystal nuclei at the early stages of crystallization due to the 1D anisotropy of the cylindrical nanopores; (ii) a continuous nucleation and growth process wherein nanocrystals with the fast-growth direction parallel (or nearly parallel) to the pores are preferred because they can achieve critical size more readily than nuclei with other alignments in which growth along the fast-growth direction would be obstructed by the pore walls. Such "misaligned" crystals would be prevented from achieving their natural habit, which reflects the balance between surface and volume free energies. As such, misaligned crystals would be less stable and more inclined to redissolve than those with their fast-growth axis aligned with the pores; (iii) (010) and (0$\bar{1}$0) faces of the two enantiomorphs are vanishingly small, suggesting that these faces have high surface energies and that the observed crystal alignment minimizes the overall surface energy of the nanocrystals. Examination of the crystal structure of β-glycine reveals multiple hydrogen bonds along ⟨010⟩, ⟨001⟩, and ⟨100⟩. Notably, the [010] direction is characterized by the greatest number of hydrogen bonds, which is consistent with large surface energies for the (010) and (0$\bar{1}$0) faces. As such, the nanoscale pores physically constrain crystal growth so that the crystal face with the highest surface energy spans the narrowest dimension of the pore. Any tilt of this face relative to the pore direction would produce an increase of the surface area of this unfavorable plane, thereby increasing the total free energy of the crystal.

Crystallization with Chiral Auxiliaries. Racemic Trp alone, quasi-racemic Phe-Trp or Met-Trp, combinations of enantiopure Phe or Met with racemic Trp, combinations of racemic Phe or Met with enantiopure Trp, and combinations of racemic Phe or Met with racemic Trp dramatically suppress growth along the ⟨010⟩ of bulk β-glycine crystals, resulting in a substantial change in the habit of the crystals from needles to plates or prismatic blocks (Figure 5A, B)[5] due to binding of the chiral auxiliaries to the {010} faces.

This behavior prompted us to examine the effect of these auxiliaries on the growth characteristics of β-glycine nanocrystals embedded in the 1D cylinders of the p-PS-PDMA monoliths by infiltrating the monoliths with solutions containing both glycine and individual auxiliaries, in concentrations comparable to those used in the prior bulk experiments. β-Glycine was then crystallized in the monoliths as described above. SEM of the porous surface of the monoliths following this treatment revealed nanocrystals protruding from the cylindrical pores, as illustrated in Figure 3B for crystals grown in the presence of *R*,*S*-phenylalanine. Notably, these crystals were substantially smaller than those observed in the absence of the auxiliaries (Figure 3A), which mirrors the changes in crystal habit observed in the bulk due to suppression along ⟨010⟩. We also note that glycine crystallization from bulk solutions (by evaporation) in the presence of racemic Phe or racemic Met results in the exclusive formation of the γ-glycine polymorph. Crystallization in the cylindrical nanopores of the PS-PDMA monoliths, however, only afforded the β polymorph, underscoring the influence of nanoconfinement on the crystallization outcome.

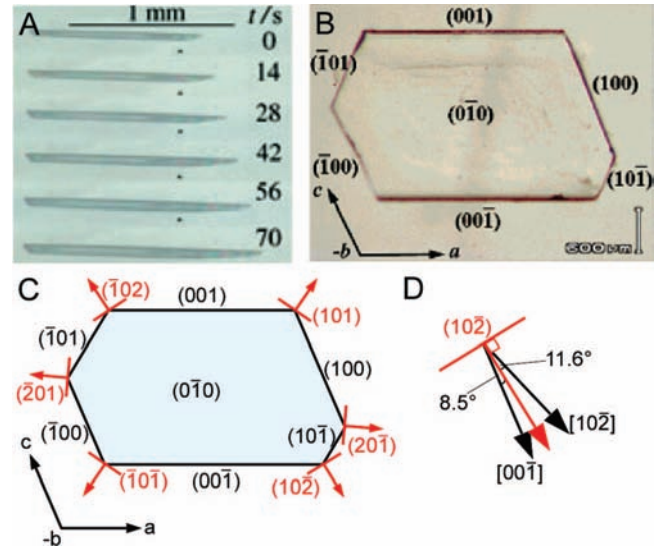

Figure 5. (A) Bulk β-glycine crystals retrieved at different times during evaporation of ethanol−water solutions containing glycine without chiral auxiliaries (Adapted with permission from ref 4. Copyright Wiley-VCH Verlag GmbH & Co. KGaA.). The long axes of the needles correspond to the ⟨010⟩ directions. (B) A bulk β-glycine crystal, grown by evaporation of an aqueous solution containing glycine and 0.3% *R*,*S*-Trp (w/w water; equivalent to 2% w/w glycine) exhibits a plate-like habit (adapted from ref 5. Copyright 2005 American Chemical Society). The crystal habit is illustrative of the habit for β-glycine crystals grown with Phe and Met auxiliaries. The large faces of the plate correspond to the {010} planes that result from the suppression of growth along ⟨010⟩ by the auxiliary. (C) Schematic representation of the β-glycine crystal in panel B illustrating the crystal faces (red) that have vanishingly small areas because of fast growth along directions (red arrows) perpendicular to their surface. Notably, X-ray diffraction reveals that the (10$\bar{2}$) plane is effectively perpendicular to the p-PS-PDMA monolith pore direction when glycine is crystallized in the presence of a racemic mixture of a chiral auxiliary (Met, Phe, Trp). (D) Illustration of the relationship between the (10$\bar{2}$) plane and the nearly perpendicular [00$\bar{1}$] and [10$\bar{2}$] directions.

The scattering patterns obtained for the embedded β-glycine nanocrystals grown in the presence of racemic mixtures of chiral auxiliaries (*R*,*S*-Phe, *R*,*S*-Met, *R*,*S*-Trp) differed significantly from those observed for β-glycine alone, signifying a change in the preferred orientation of the nanocrystals (Figure 6). The Bragg reflections were characterized by arcs of intensity, with the azimuthal spread comparable to that described above for β-glycine alone, with (001), (020), and (10$\bar{2}$) exhibiting measurable intensities over the ranges $20° \le \delta \le 40°$, $74° \le \delta \le 106°$, and $-16° \le \delta \le 16°$, respectively. Analysis of the scattering pattern revealed that the (10$\bar{2}$) plane was perpendicular to the cylindrical pore (Table 2). Under the monoclinic symmetry of β-glycine, the [10$\bar{5}$] direction is perpendicular to this plane and thus would coincide with the pore direction. The [001] axis and [10$\bar{2}$] directions, however, are nearly perpendicular to (10$\bar{2}$), at 8.5° and 11.6° from the plane normal, respectively. Moreover, the data reveal the {010} planes were now parallel to the cylinder direction, corresponding to ⟨010⟩ directions perpendicular to the cylinder direction, a 90° "flip" compared with the orientation in the absence of auxiliaries.

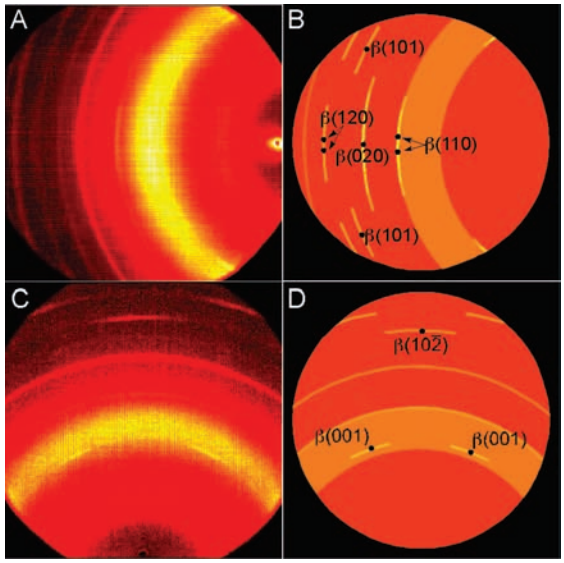

Figure 6. Diffraction patterns for β-glycine nanocrystals, grown by evaporation of aqueous solutions containing 18% glycine (w/w water) and 1.2% *R*,*S*-Phe (w/w water), embedded within the 22-nm cylindrical pores of a p-PS-PDMA monolith. Similar diffraction patterns are observed for β-glycine nanocrystals grown in the presence of *R*,*S*-Met and *R*,*S*-Trp. (A) The left quadrant of the 2D detector ($45° \leq 2\theta \leq 135°$) reveals arcs of intensity due to Bragg reflections. (B) A schematic enhancing the reflection positions and locations of maximum intensity in panel A with the corresponding assignments. (C) Top quadrant of the 2D detector ($-45° \leq 2\theta \leq 45°$) with the monolith fixed in the same configuration. (D) A schematic enhancing the reflection positions and locations of maximum intensity in panel A with the corresponding assignments. The orientation of the Bragg reflections and monolith channels suggests the [00$\bar{1}$] directions of β-glycine grow nearly parallel to the pore direction. The schematics B and D were constructed using the raw data as a guide with the intent of clarifying the Bragg reflection assignments and positions in the raw data. The black dots denote the azimuthal angle corresponding to maximum intensity. Some reflections exhibit intensity maxima at two azimuthal angles, related by symmetry, corresponding to opposite orientations of the crystals in the monolith pores (see Table 3).

Combinations of a racemic mixture of a chiral auxiliary (*R*,*S*-Met or *R*,*S*-Phe) with an enantiopure or racemic mixture of Trp afforded similar results. In contrast, the scattering patterns obtained for the embedded β-glycine nanocrystals grown in the presence of enantiopure chiral auxiliaries (*R*- or *S*- Phe, Met, or Trp; Table 3), which should only impede the growth of one of the β-glycine enantiomorphs, were identical to those observed for β-glycine alone.

Examination of the crystal structure of β-glycine reveals multiple hydrogen bonds along ⟨010⟩, ⟨001⟩, and ⟨100⟩. The interruption of growth along ⟨010⟩ by racemic auxiliaries would be expected to favor growth along other hydrogen-bonding directions, in this case ⟨001⟩, which lies in {010} and is nearly perpendicular to (10$\bar{2}$). The (10$\bar{2}$) can be described as having a high surface energy because it truncates the ⟨001⟩ hydrogen bonds. This high surface energy would forecast a small area for this face and fast growth perpendicular to its surface so that the overall surface energy is minimized as the crystal volume expands. This is consistent with bulk β-glycine crystals grown in the presence of racemic mixtures of chiral auxiliaries, where the (10$\bar{2}$) face is vanishingly small, corresponding to a corner intersected by the (00$\bar{1}$) and (10$\bar{1}$) planes (Figure 5C). Therefore, this crystal alignment under confinement minimizes the overall surface energy of the nanocrystals, apparently overcoming any favorable volume free energy due to growth along the ⟨010⟩ directions. As with the ⟨010⟩ alignment for crystallization without auxiliaries, the nanoscale pores physically constrain crystal growth so that the crystal face with the higher surface energy spans the narrowest dimension of the pore. Any tilt of this face relative to the perpendicular to the pore direction results in an increase of the surface area of this unfavorable plane, thereby increasing the total free energy of the crystal, all other factors being equal. For β-glycine embedded within p-PS-PDMA, this attempt to minimize the surface area of (10$\bar{2}$) results in [10$\bar{5}$] aligned parallel to the pore direction and [001], the fast growth direction, aligned very nearly parallel to the pore direction (Figure 5D). We also note that the observation of two different alignments for crystals grown in the absence and presence of auxiliaries argues that heterogeneous nucleation on the pore walls, involving a favorable interaction with a specific set of crystal planes of emerging nuclei, has little influence on the crystallization process.

Table 2. The Measured and Expected δ Values for Glycine Nanocrystals Grown in the Monoliths with *R*,*S*-Phenylalanine Auxiliaries. The (10$\bar{2}$) Crystal Plane Was Preferentially Aligned Perpendicular to the Pore Direction

	measured				expected		
reflection (*hkl*)	2θ (deg)	δ (deg)[a]	cos θ cos δ	ϕ (deg)[b]	2θ (deg)	ϕ (deg)[c]	δ (deg)[a,b]
(001)	17.9	30, 150	0.82	35	17.9	31.6	30, 150
(110)	23.8	90	0.00	90	23.8	83.2	83, 97
(020)	28.5	90	0.00	90	28.5	90	90
(101)	31.1	69, 121	0.31	72	31.0	66	65, 115
(10$\bar{2}$)	33.7	0[d]	0.83	17[d]	33.7	0[d]	*d*
(021)	33.8	60, 120	0.42	65	33.8	62.8	61, 119
(120)	34.3	85, 95	0.07	86	34.4	85.3	85, 95
(12$\bar{1}$)	36.6	60, 120	0.42	65	36.3	58.8	57, 123
(11$\bar{2}$)	36.6	N/A[e]	–	–	36.7	23	14, 166

[a] Reflections appearing as pairs of δ values were caused by glycine nanocrystals oriented in opposite directions within the pores, where the symmetry between the crystal orientations resulted in reflections mirrored across $\delta = 0°$ and 90°. [b] Calculated using eq 3a. [c] Calculated from (*hkl*) and (10$\bar{2}$). The [001] is assumed to be the fast-growth direction and is nearly parallel to the pore direction. [d] ϕ (from measured) is the apparent angle between (hkl) and (10$\bar{2}$), the plane perpendicular to the pore direction. The (10$\bar{2}$) is parallel to the beam, and only forward scattering would be expected from this plane, that is, there would be no reflection expected for the (10$\bar{2}$). The crystals are not all perfectly aligned, however, and the small fraction of crystals oriented such that their (10$\bar{2}$) is tilted ($2\theta/2$) $\theta = 16.85°$ relative to the beam satisfy the Bragg condition. This leads to the appearance of the (10$\bar{2}$) reflection at $\delta = 0°$, which corresponds to an apparent $\phi = \theta = 16.85°$. [e] Reflection not observed in the data.

Collectively, these observations reveal a correspondence between the effect of chiral auxiliaries on the growth of bulk β-glycine and embedded β-glycine nanocrystals and a connection between the fast growth direction of β-glycine nanocrystals and their orientation in the cylindrical pores. In the absence of auxiliaries the nanocrystals grow with their native fast growth direction, ⟨010⟩, aligned with the cylindrical pore. This suggests that "misaligned" nuclei, with ⟨010⟩ axes inclined to the pore direction, are disfavored because their growth is obstructed by the pore walls, with fewer achieving critical size during crystallization compared with those with ⟨010⟩ aligned along the pore direction. The suppression of these misaligned nuclei would diminish as ⟨010⟩ approaches an alignment coinciding with the pore direction, which is consistent with the distribution of orientations evident from the arcs of intensity about central maxima for the Bragg reflections. The addition of racemic auxiliaries, however, alters the relative kinetics of growth along the various crystallographic directions, suppressing growth along

Table 3. The Effect of Chiral Auxiliaries on the Orientation of β-Glycine Nanocrystals Embedded in p-PS-PDMA

auxiliary 1[a]	(% w/w water)	(% w/w gly)[b]	auxiliary 2[a]	(% w/w water)	(% w/w gly)[b]	β-glycine crystal direction parallel to pore direction[c]
none	–	–	–	–	–	[010]
R- or *S*-Phe	1.2	8	–	–	–	[010]
R- or *S*-Met	1.2	8	–	–	–	[010]
R- or *S*-Trp	0.3	2	–	–	–	[010]
R,*S*-Met	0.6−1.2	4−8	–	–	–	[00$\bar{1}$]
R,*S*-Phe	0.6−1.2	4−8	–	–	–	[00$\bar{1}$]
R,*S*-Trp	0.3	2	–	–	–	[00$\bar{1}$]
R,*S*-Met	1.2	8	*R*,*S*-Trp	0.3	2	[00$\bar{1}$]
R,*S*-Met	1.2	8	*R*- or *S*-Trp	0.3	2	[00$\bar{1}$]
R,*S*-Phe	1.2	8	*R*,*S*-Trp	0.3	2	[00$\bar{1}$]
R,*S*-Phe	1.2	8	*R*- or *S*-Trp	0.3	2	[00$\bar{1}$]

[a] The auxiliary abbreviations are Phe (phenylalanine), Met (methionine), and Trp (tryptophan). [b] The aqueous solutions contained 18% glycine (w/w water). [c] The glycine crystals grown from aqueous solutions containing glycine and racemic mixtures of amino acids resulted in crystals with (10$\bar{2}$) perpendicular to the pore direction, with [00$\bar{1}$], which was a strong hydrogen bonding direction in β-glycine and the fast-growth direction, nearly parallel to the pores (within 8.5°).

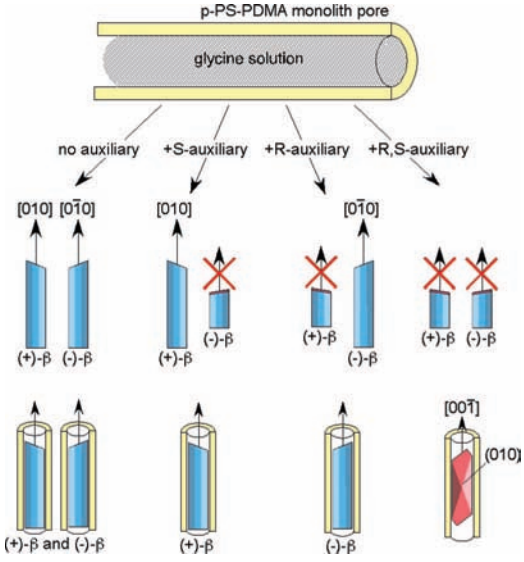

Figure 7. Preferred orientations adopted by β-glycine nanocrystals grown within p-PS-PDMA in the presence of no, enantiopure, and racemic mixtures of chiral auxiliaries.

⟨010⟩ such that growth along another crystallographic direction is preferred, in this case the ⟨001⟩.

Notably, because β-glycine is chiral and exists as two enantiomorphs, an enantiopure chiral auxiliary binds selectively to a particular face of only one of the enantiomorphs, in this case the (010) of (+)-β or the (0$\bar{1}$0) of (−)-β, depending on the handedness of the auxiliary.[25] Under these conditions, the enantiopure auxiliary will inhibit the growth of only one of the enantiomorphs, allowing the other to grow unimpeded with characteristics identical with those observed for in the absence of any stereochemical inhibitor. For example, *S*-Trp, *S*-Met, and *S*-Phe selectively inhibit growth along the <0$\bar{1}$0> direction for (−)-β-glycine by binding to the (0$\bar{1}$0) face.[4] Because growth of the (+)-β enantiomorph is not affected these crystals grow normally along the [010] direction, such that the (+)-β nanocrystals are oriented with [010] parallel to the pore direction (Figure 7).

Concluding Remarks

These results demonstrate that β-glycine crystals, which are favored under nanoscale confinement, adopt an orientation in which the fast-growth direction is aligned with the pore direction. The addition of a racemic mixture of chiral auxiliaries, which inhibits growth along the native fast-growth direction, generates a different orientation. These observations argue against heterogeneous nucleation wherein a particular crystal plane interacts favorably with the pore walls. Instead, the results suggest that the observed orientations are a consequence of critical size effects and surface energy considerations, wherein confinement favors growth orientations that permit nuclei to achieve critical size more competitively when their fast-growth axis is unimpeded by pore walls and the area of the face with the highest surface energy is minimized when aligned perpendicular to the pore. Collectively, these observations illustrate the connection between bulk crystal habit and nanocrystal orientation under size confinement. The ability to manipulate the orientation of nanocrystals under extreme size confinement could provide new routes to composite materials while enabling exploration of the structure−property relationships at the nanoscale, for example, solid-state reactions occurring in organic nanocrystals with dimensions smaller than those reported previously.[26,27] It is also interesting to consider whether the formation of a noncentrosymmetric crystalline phase because of nanoconfinement—in this case β-glycine, the simplest amino acid—suggests a role for this phenomenon in the genesis or amplification of biological homochirality in clay or mineral matrices.[28]

Acknowledgment. This work was supported primarily by the Binational Science Foundation and the MRSEC Program of the National Science Foundation (under Award Numbers DMR-0212302 and DMR-0819885 at the University of Minnesota and under Award Number DMR-0820341 at New York University). Portions of this work were performed in the University of Minnesota I.T. Characterization Facility, which receives partial support from NSF through the NNIN program. The authors are grateful to Mr. Brian Olmsted for helpful comments.

JA807193S

(25) The range of orientations exhibited by the β-glycine nanocrystals embedded in p-PS-PDMA precluded the determination of their chirality from any of the 2-D m-XRD data.

(26) Takahashi, S.; Miura, H.; Kasai, H.; Okada, S.; Oikawa, H.; Nakanishi, H. *J. Am. Chem. Soc.* **2002**, *124*, 10944–10945.
(27) Bucăr, D.-K.; MacGillivray, L. R. *J. Am. Chem. Soc.* **2007**, *129*, 32–33.
(28) (a) Weissbuch, I.; Leiserowitz, L.; Lahav, M. *Top. Curr. Chem.* **2005**, *259*, 123–165. (b) Castro-Puyana, M.; Salgado, A.; Hazen, R. M.; Crego, A. L.; Alegre, M. L. M. *Electrophoresis* **2008**, *29*, 1548–1555. (c) Hazen, R. M.; Sholl, D. S. *Nat. Mater.* **2003**, *2*, 367–374. (d) Hazen, R. M.; Filley, T. R.; Goodfriend, G. A. *Proc. Natl. Acad. Sci.U.S.A.* **2001**, *98*, 5487–5490.